View Article Online / Journal Homepage / Table of Contents for this issue

Anodic behaviour of methylidene-cyclopentadiaryl derivatives: cyclic voltammetry and theoretical study†‡

Cécile Hubert,[a] Khoa Tran,[a] Fanny Hauquier,[a] Charles Cougnon,[a] Jean-François Pilard,*[a] Pascal Gosselin,*[a] Joëlle Rault-Berthelot[b] and Eugène Raoult[b]

Received (in Montpellier, France) 21st March 2007, Accepted 4th June 2007
First published as an Advance Article on the web 28th June 2007
DOI: 10.1039/b704340f

Published on 28 June 2007 on http://pubs.rsc.org | doi:10.1039/B704340F
Downloaded by University of Belgrade on 01 January 2013

Electrochemical behaviour of a functionalized fluorenylidene **1** is studied in comparison with a cyclopentadithiophene analogue **2**. The influence of the main aromatic group on the electropolymerization ability is reported. We demonstrated that the lack of sulfur atoms in the monomer structure leads to an absence of polymerization due to the spin density located on the methylidene bridge in the radical cation. From modelling considerations, we have evaluated the participation of the methylidene bridge in the p-doping process. The good correlation between the p-doping level and the partial atomic charge carried by the methylidene bridge for poly(**2**) and poly(**3**) indicates that an extension of the conjugated area improves the p-doping level when the side chain is electronically connected to the main chain of polymer.

Introduction

Among the wide class of conjugated matrixes developed in the past decade, polyfluorenes have been of growing interest in the development of various electronic devices such as LED's, sensors or solid-state lasers.[1,2] These polymers exhibit a strong thermal stability and high photo- and electroluminescence efficiencies both in solution and in the solid state. In addition, the introduction of a substituted methylidene group at the bridge position has attracted special attention for low band-gap materials[3] and could potentially be used in electronic devices. Herein, we report our preliminary results on conducting polymers suitable for electrochemical applications such as cathodic drug delivery.[4] Indeed, in a previous work, we reported the remarkable electroactivity of a conducting poly(cyclopentadithiophene) matrix, named poly(**2**), electronically connected to an electro-sensitive group *via* a conjugated spacer.[5] The study of a polyfluorenylidene analogue, poly(**1**), might be of great interest for biosensor applications. Nevertheless, the anodic behaviour of compounds **1** and **2** appears different. Whereas **2** leads to a polymer *via* a classical anodic oxidation, no radical cation coupling occurs after oxidation of **1**.

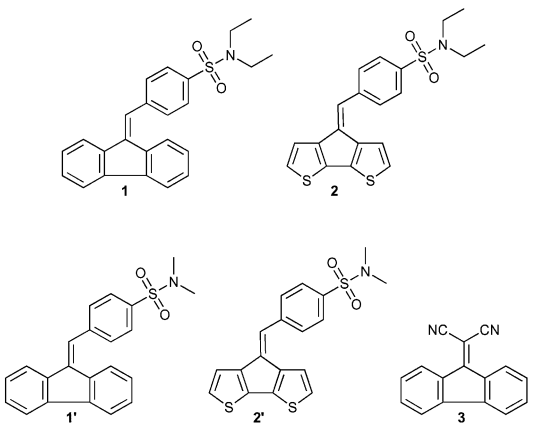

In order to understand the origin of the difference in behaviour between the two compounds and to explain the polymerization process of **2**, we performed DFT *ab initio* calculations on the parent compounds **1′** and **2′** of **1** and **2**. Furthermore, the easily electropolymerizable 2-(9*H*-fluoren-9-ylidene)malononitrile **3** [6] was also studied.

Experimental

Monomer synthesis

All reactions were carried out under nitrogen atmosphere. All organic solvents were distilled prior to use and all chemicals reagents were used as received. ^{1}H NMR Spectra were recorded on a Bruker AC 400 spectrometer and chemical shifts are reported in ppm downfield from tetramethylsilane (multiplicity; s: singlet, d: doublet, t: triplet, q: quadruplet and

[a] *Unité de Chimie Organique Moléculaire et Macromoléculaire (UCO2M, UMR CNRS 6011), Université du Maine, Avenue O. Messiaen, F-72085 Le Mans, France. E-mail: jean-francois.pilard@univ-lemans.fr. E-mail: pascal.gosselin@univ-lemans.fr; Fax: +33 2438 33754; Tel: +33 2438 33540*
[b] *Laboratoire d'Electrochimie Moléculaire & Macromoléculaire (UMR CNRS 6510), Institut de Chimie de Rennes, Université de Rennes I, 263 Avenue du Général Leclerc, F-35042 Rennes, France*

† The HTML version of this article has been enhanced with additional colour images.

‡ Electronic supplementary information (ESI) available: Optimized Cartesian coordinates and corresponding energies for **1′**, **2′** and **3** (both neutral and radical cation species). Complete listing of Mulliken and NPA spin densities and of CHelpG, NPA and MKS charges. See DOI: 10.1039/b704340f

 This journal is © the Royal Society of Chemistry and the Centre National de la Recherche Scientifique 2007

Published on 28 June 2007 on http://pubs.rsc.org | doi:10.1039/B704340F
Downloaded by University of Belgrade on 01 January 2013

m: multiplet, integration and peak assignments). Monomer **1** was synthesized by a Wittig reaction and monomer **2** was prepared by condensation of 4*H*-cyclopenta[2,1-*b*:3,4-*b*′]dithiophene (CPDT) with *p*-(*N*,*N*-diethylsulfamoyl)-benzaldehyde.

9-(4-(*N*,*N*-Diethylsulfamoyl)benzylidene)-9*H*-fluorene 1

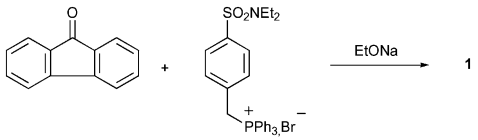

The phosphonium salt was obtained from a mixture of *p*-(*N*,*N*-diethylsulfamoyl)benzyl bromide (0.5 mmol) and triphenylphosphine (1.07 eq.) in anhydrous DMF (1.3 cm^3). After 20 min stirring at 130 °C, the solution was cooled at room temperature and the solvent was evaporated under reduced pressure. For preparation of monomer **1**, EtONa (1 eq.) was added at 60 °C to an absolute ethanol solution (2.5 cm^3) containing the phosphonium salt (0.5 mmol) and fluorenone (1 eq.), and the reaction was refluxed for 3 h. Next, the mixture was cooled at room temperature, hydrolyzed with 6 cm^3 of water and extracted with CH_2Cl_2. The organic phase was washed with water, dried with $MgSO_4$ and evaporated. Chromatography of the residue (SiO_2, petroleum ether–CH_2Cl_2 1 : 1) afforded the title compound with a side-product corresponding to 1-(*p*-toluenesulfonyl)diethylamine. Preparative HPLC purification (μPorasil 10 μm 125 Å, PrepPak Cartridge 40 × 100 mm column) was necessary to obtain pure monomer **1** (56 mg, 30%) as a yellow powder: mp 117.3–117.6 °C; δ_H (400 MHz; $CDCl_3$; Me_4Si) 1.18 (6 H, t, *J* 7.2, 2 × CH_3), 3.32 (4 H, q, *J* 7.2, 2 × CH_2N), 7.04 (1 H, m, $H_{fluorene}$), 7.30–7.41 (4 H, m, $H_{fluorene}$), 7.60 (1 H, s, $H_{vinylic}$), 7.68–7.69 (2 H, m, H_{phenyl}), 7.70–7.71 (2 H, m, $H_{fluorene}$), 7.76 (1 H, d, *J* 8.4, $H_{fluorene}$) and 7.89 (2 H, br d, *J* 8.3, H_{phenyl}); δ_C (100 MHz; CDCl3) 14.25 (q, *C*H_3), 42.18 (t, *C*H_2N), 124.86 (d, *C*H vinylic), 127.36, 130.04 (d, *C*H phenyl), 119.89, 120.12, 120.58, 124.46, 127.00, 128.98, 129.32 (d, *C*H fluorene) and 136.14, 138.32, 139.14, 139.54, 139.86, 141.41, 141.71 (s). *m*/*z* (NH_3 DCI) 390.1533 (MH^+ $C_{24}H_{24}NO_2S$ requires 390.1528).

4-(4-(*N*,*N*-Diethylsulfamoyl)benzylidene)-4*H*-cyclopenta-[2,1-*b*;3,4-*b*′]dithiophene 2

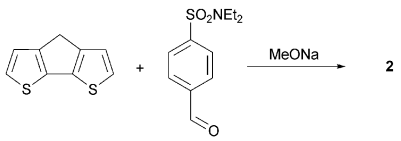

MeONa (1.2 mmol) was added dropwise to a MeOH solution (2.1 cm^3) containing CPDT (110 mg, 0.62 mmol). After stirring at room temperature during 30 min, a solution of *p*-(*N*,*N*-diethylsulfamoyl)benzaldehyde (0.63 mmol) in MeOH (4.2 cm^3) was added and the reaction refluxed for 2 h. Next, the mixture was cooled to room temperature, hydrolyzed with distilled water and extracted with CH_2Cl_2. The organic phase was washed with water and after drying with $MgSO_4$, the solvent was evaporated. Chromatography of the residue (SiO_2, CH_2Cl_2–*n*-pentane 7 : 3) afforded the title compound (100 mg, 40% yield) as a red powder: mp 159–163 °C; δ_H (400 MHz; $CDCl_3$; Me_4Si) 1.17 (6 H, t, *J* 7.2, 2 × CH_3), 3.30 (4 H, q, *J* 7.2, 2 × CH_2N), 6.95 (2 H, m, $H_{thiophene}$), 7.12–7.20 (2 H, m, $H_{thiophene}$), 7.26 (1 H, s, $H_{vinylic}$) and 7.69–7.88 (4 H, m, H_{phenyl}); δ_C (100 MHz; CDCl3) 14.33 (q, *C*H_3), 42.24 (t, *C*H_2N), 119.96, 122.86, 124.45, 125.36 (d, *C*H thiophene), 126.41 (d, *C*H vinylic), 127.21, 130.31 (d, *C*H phenyl) and 132.87, 137.79, 140.04, 140.76, 141.71, 141.73, 146.92 (s); *m*/*z* (NH_3 DCI) 402.0667 (MH^+ $C_{20}H_{20}NO_2S_3$ requires 402.0656).

Electrochemical experiments and instrumentation

Bu_4NPF_6 was purchased from Fluka and used as received (electrochemical grade). The salt was stored in a desiccator over silica gel. Acetonitrile purchased from SDS was used without any further purification and stored under an argon atmosphere. Electrochemical experiments were performed under an argon atmosphere, in a three-electrode cell constituted of a platinum disk (id = 1 mm) as working electrode, a vitreous carbon rod as counter electrode and a silver wire immersed in a 0.1 M $AgNO_3$ acetonitrile solution used as reference electrode. Ferrocene was added to the electrolyte solution at the end of a series of experiments. The ferrocene/ferrocenium system was used as internal standard and all reported potentials were referred to its reversible formal potential. The cell was connected to an EG&G PAR Model 173 potentiostat monitored with an EG&G PAR Model 175 signal generator and an EG&G PAR Model 179 digital coulometer.

Computational details

Geometries of compounds **1**′ and **2**′ were optimized as follow: a Monte Carlo conformer distribution analysis was first performed within MacSpartan'02 [7] at the AM1 level of theory for the neutral molecules. The most stable conformer was then subjected to geometry optimization under no constraints at the DFT level within Gaussian98.[8] The DFT calculations on neutral molecules were carried out using the RB3LYP hybrid functionals. In order to examine the impact of a larger basis set on both the geometry and the electronic properties, the CPDT analogue **2**′ was first studied with both the 6-31G(d) and the 6-31 + G(d,p) basis sets. However, similar results were obtained with both basis sets (see thereafter) and subsequent calculations were only performed with the 6-31G(d) basis set. These optimized structures of the neutral compounds were used as the starting point of the geometry optimization of the corresponding radical cations at the UB3LYP/6-31G(d) level (and also UB3LYP/6-31G + (d,p) for **2**′ radical cation). In all cases, the default convergence criteria were kept and the stability of the wavefunction was ascertained (Stable keyword). The maximum value of S^2 obtained for the radical cations was 0.77, very close to the value of 0.75 theoretically required for a doublet (*i.e.* spin contamination is almost absent).

Results and discussion

Comparative anodic oxidation of 1 and 2

The anodic behaviour of monomer **2** in acetonitrile solution containing 0.1 M Bu_4NPF_6 is shown in Fig. 1. As expected for

Published on 28 June 2007 on http://pubs.rsc.org | doi:10.1039/B704340F
Downloaded by University of Belgrade on 01 January 2013

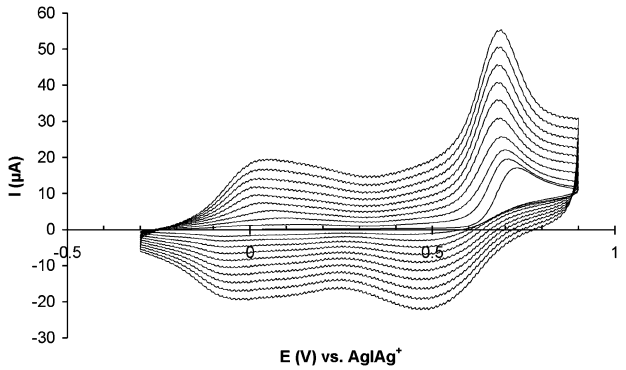

Fig. 1 Polymerization of **2**.

modified cyclopentadithiophene compounds, after oxidation up to the first anodic wave, a new redox system appears and increases regularly at less positive potential along recurrent sweeps. This reversible system corresponding to the p-doping process of the polymer chains at the electrode surface increases in intensity according to the growth of an electroactive film at the electrode with the recurrent sweep of potential.

After the formation of the film, the electrode is rinsed in acetonitrile and used in a monomer-free acetonitrile solution. A characteristic CV is shown in Fig. 2 and is ascribed to the p-doping process of poly(**2**).

The anodic behaviour of modified fluorenylidene **1** in acetonitrile solution is shown in Fig. 3. Two irreversible waves are observed at +1.3 V and +1.8 V (Fig. 3A). Whatever the reverse potential location, subsequent CV's lead to a decrease of current in accordance with an inhibition process (Fig. 3B–C).

Computational calculations on 1′, 2′ and 3

In order to account for the contrasting behaviour of **1** *vs.* **2**, we thus undertook a DFT study of both neutral molecules as well as their radical cations. Besides, to gain insight into the origin of the different behaviour of 1 *vs.* 2-(9*H*-fluoren-9-ylidene) malononitrile **3**,[6] the latter was also studied. As a minor simplification, the dimethylsulfonamides **1′** and **2′** were studied instead of the diethyl compounds.

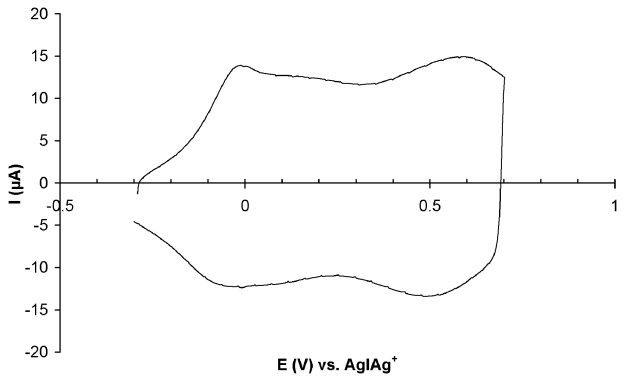

Fig. 2 Cyclic voltammograms recorded on a poly(**2**)-coated platinum electrode in an acetonitrile monomer-free solution containing 0.1 M Bu_4NPF_6 used as support salt. Scan rate: 100 mV s^{-1}.

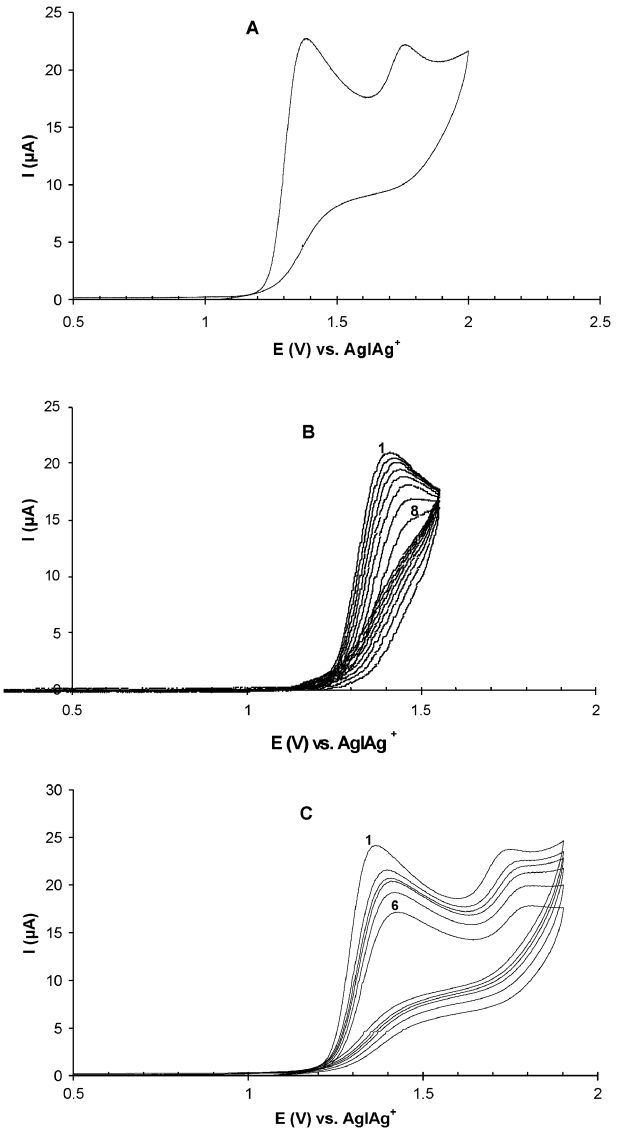

Fig. 3 Anodic oxidation of **1**.

Since the pioneering work of Diaz *et al.* on polypyrrole,[9] the so called RC–RC (radical cation–radical cation) mechanism of electropolymerization of aromatic monomers is now generally accepted.[10] According to this mechanism (Scheme 1), the first step involves the formation of cationic radicals which then evolve by radical coupling to form a dimer dication.[11–18] The driving force of the subsequent elimination of two protons is the restoration of an aromatic system within the dimer. That dimer then undergoes oxidation and the whole process is thereupon repeated. The concurrent RC–S (radical cation–substrate) mechanism, which involves the reaction between a radical cation and a neutral substrate molecule, was also proposed.[19–22] However, recent modelling studies indicate that the oxidative polymerization of aromatic heterocyclic monomers is more likely to occur *via* the RC–RC mechanism.[14,17,18,23]

Various modelling approaches of the electropolymerization reaction *via* radical coupling of radical cations have been developed in recent years. Most of them only pertain to the

 This journal is © the Royal Society of Chemistry and the Centre National de la Recherche Scientifique 2007

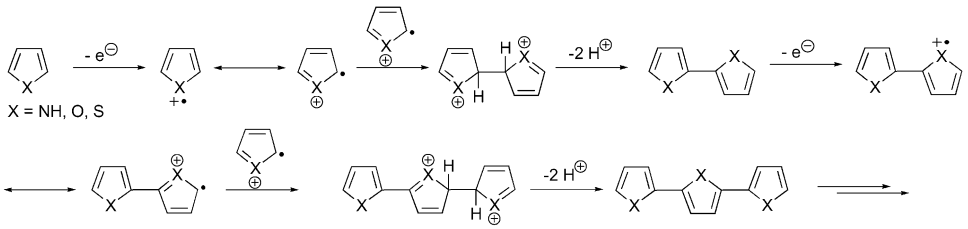

Scheme 1 Mechanism of electropolymerization *via* RC–RC coupling.

Published on 28 June 2007 on http://pubs.rsc.org | doi:10.1039/B704340F
Downloaded by University of Belgrade on 01 January 2013

first stage of the polymerization process *i.e.* the formation of the dimer. Besides FMO (Frontier Molecular Orbitals) treatments,[14,24–26] some recent studies focus on energetics of the successive steps,[17,23] transition state calculations[10,14,18] or take advantage of the softness–hardness concept.[27]

Meanwhile, as early as 1969, Adams pointed out the unpaired electron density localization as a valuable reactivity index for a radical cation.[28] Coupling is more likely to occur at the position of highest unpaired electron spin density. This constitutes a handy way to quickly estimate both the regioselectivity and ease of the polymerization process. Although significant results were obtained with semi-empirical methods on simple representatives of various classes of aromatic monomers,[11,13,29–36] Density Functional Theory (DFT) methods are now highly regarded due to their excellent effectiveness/computational cost ratio. Since 1995,[12] this technique has been successfully used to determine precisely the spin densities of various monomer radical cations including N-heteroaryls,[12,37–40] S-heteroaryls[12,15,16,38,41] and aryl compounds.[27]

Study of the structural changes occurring in the monomers following the one-electron oxidation. More than the bond lengths themselves, the *variations* of bond lengths between the neutral molecule and the radical cation are instructive. These variations correspond to the difference in the bond lengths in the radical cation and the bond lengths in the neutral molecule. A positive variation corresponds to an increase in the bond length and *vice versa*. Fig. 4 displays these variations expressed in mÅ for **1′**, **2′** and **3**.

The variation of bond lengths for **1′** suggests that the whole molecule is perturbed by the formation of the radical cation. The most important variation of bond length in **1′** concerns the methylidene bridge C^7–C^{14} which increases by 44 mÅ. This increase may correspond to the transformation of this double bond into a single bond in the radical cation. The propagation of the modification on the whole molecule may be in accordance with the mesomeric structures depicted in Scheme 2.

Starting from the radical cation **a**, a quinoid structure appears on the benzenesulfonamide group, implying a strong shortening of the C^{14}–C^{15} bond (−41 mÅ). On the other hand, in the "regioisomeric" radical cation **a′**, the quinoid structure concerns the fluorene part which is reflected in the shortening of C^4–C^7 and C^7–C^8 bonds. A trend that emerges from these bond length variation calculations on **1′** is that both benzenesulfonyl and fluorenyl aromatic systems are perturbed by the formation of the cation radical.

The dihedral angles in the radical cation of **1′** greatly differ from those computed for the neutral form **1′** (Table 1) showing a great change in the structure of the molecule upon oxidation. The 42° C^7–C^{14}–C^{15}–C^{16} dihedral angle computed for neutral **1′** becomes 21.5° in the radical cation. A *ca.* 20° flattening of this dihedral angle is computed for the radical cation of **1′** with a concomitant 12.5° twist of the C^4–C^7–C^{14}–H dihedral angle. This last twist may be easily interpreted by the loss of the double bond character of the methylidene bridge in agreement with all canonical forms shown in Scheme 2. The flattening of the C^7–C^{14}–C^{15}–C^{16} dihedral angle could reflect the emergence of a double bond character for the C^{14}–C^{15} bond, implying the significant contribution of mesomers **b** and **c** (Scheme 2) to the resonance hybrid and consequently, a smaller contribution of mesomer structure **a′** to the "real" radical cation in comparison with **a**.

With **2′**, the greatest bond length contraction (−52 mÅ) involves the C^1–C^6 bond while important lengthenings involve C^1–C^2 (+48 mÅ) and C^6–C^7 (+47 mÅ) bonds (Fig. 4). A bond length contraction obviously reflects the increase of double bond character for the C^1–C^6 bond in the radical cation, while the lengthening of the C^1–C^2 and C^6–C^7 bonds indicates a loss of double bond character when going from the neutral molecule to the radical cation. These results are fully in

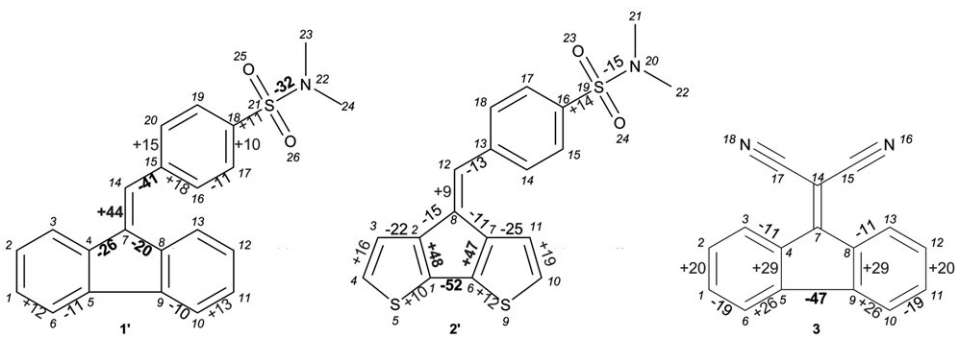

Fig. 4 Computed variations (mÅ, B3LYP/6-31G(d)) of bond lengths between the radical cations of **1′**, **2′** and **3** and their neutral forms. B3LYP/6-31G+(d,p) calculations only differ by ±2 mÅ. Variations smaller than + or −10 mÅ are not reported.

View Article Online

Published on 28 June 2007 on http://pubs.rsc.org | doi:10.1039/B704340F
Downloaded by University of Belgrade on 01 January 2013

Table 1 Selected computed dihedral angles in **1′** (°, B3LYP/6-31G(d))

Dihedral	C^7–C^{14}–C^{15}–C^{16}	C^4–C^7–C^{14}–H
1′ Neutral (N)	42.1	7.0
1′ Radical cation (RC)	21.6	19.5
Difference (RC − N)	−20.5	+12.4

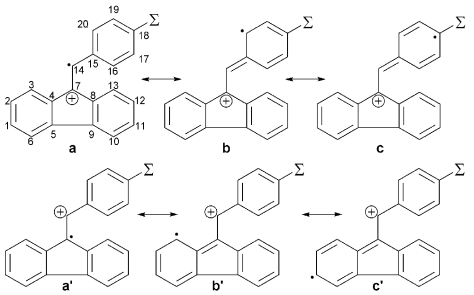

Scheme 2 Resonance structures of the radical cation of **1′** (Σ:$SO_2N(CH_3)_2$).

accordance with the different mesomers which describe together the electronic distribution for the radical cation of **2′**, as depicted in Scheme 3.

The structures of the distonic radical cation mesomers **b**–**f** reflect the main calculated bond lengths variations: the C^1–C^6 bond is always double, the symmetrical C^1–C^2 and C^6–C^7 bonds are always single while the C^4–C^5, C^7–C^{11} and C^{10}–C^{11} (and symmetrically, the C^9–C^{10}, C^2–C^3 and C^3–C^4) bonds are either single or double according to the mesomer, implying a moderate variation of their length. Whatever the mesomer considered, symmetrical C^1–S^5 and C^6–S^9 bonds are always single which is reflected by a small positive variation. Contrary to the **1′** radical cation, the C^8–C^{12} linker only exhibits a small lengthening (+9 mÅ) correlated with a limited loss of double bond character (mesomer **f**). Finally, it should be stressed that the benzenesulfonamide moiety is hardly affected by the formation of the radical cation.

The structures of **2′** and of its radical cation are not planar. In either case, the benzenesulfonamide moieties are twisted by an angle of *ca.* 35° for the C^8–C^{12}–C^{13}–C^{14} dihedral angle (Table 2 and Fig. 4). The fact that this dihedral angle remained almost unchanged in the radical cation suggest that the double bond character of the central C^8–C^{12} bond is retained in the

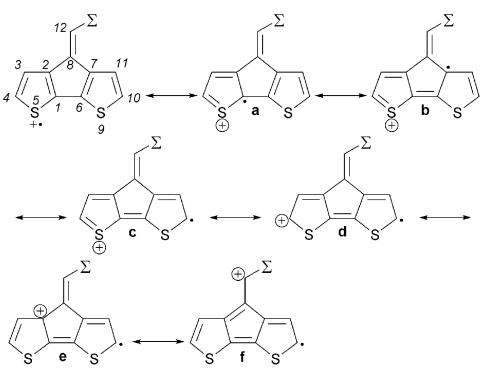

Scheme 3 Resonance structures of the radical cation of **2′** (Σ:$SO_2N(CH_3)_2$).

Table 2 Selected computed dihedral angles in **2′** (°, B3LYP/6-31G(d))

Dihedral	C^8–C^{12}–C^{13}–C^{14}	C^2–C^8–C^{12}–H
2′ Neutral (N)	36.6	6.2
2′ Radical cation (RC)	33.9	7.2
Difference (RC − N)	−2.8	+1.0

latter, in agreement with a resonance hybrid of the **a**–**e** mesomers (Scheme 3).

The strong electron-attracting effect of the cyano groups in **3** is reflected by the lengthening (*i.e.* loss of double bond character) of the C^7–C^{14} double bond in neutral **3** (1.375 Å) when compared to the equivalent double bond in both **1′** and **2′** (1.355 Å). In striking contrast with **1′**, results for 2-(9*H*-fluoren-9-ylidene)malononitrile **3** show that the C^5–C^9 bond is the most shortened upon one-electron oxidation (−47 mÅ, Fig. 4). This value is very similar to that computed for the equivalent C^1–C^6 bond in **2′** (−52 mÅ). Likewise, the C^7–C^{14} double bond is weakly affected (−4 mÅ) in **3** as in **2′** (+9 mÅ), while it is the most elongated in **1′** (+44 mÅ). These similarities between computed variations of bond lengths in **2′** and **3** lead to the conclusion that the radical cation of **3** is better represented by resonance structures located on the fluorene system, as specified in Scheme 4.

This comparative study of the geometry of both neutral molecules and radical cations of **1′**, **2′** and **3** sheds light on the origin of the contrasting behavior of **2′** (and **3**) *vs.* **1′**: on the one hand, the radical is essentially localized on the tricyclic aromatic system of **2′** and **3**, on the other hand the radical in the **1′** radical cation seems to be delocalized on the whole structure.

Study of the spin density and charge distribution of the radical cations. A graphical representation of the spin density distribution over the different radical cations is shown in Fig. 5. Table 3 depicts both the computed Mulliken[42] spin densities and the *variations* of the partial charges on individual atoms upon one electron oxidation of the neutral molecule, computed according to the CHelpG scheme.[43,44]

In the case of compound **1′**, the unpaired electron spin density for the radical cation appears distributed over the whole structure. However, the spin density found on the carbons C^{14} and C^7 shows that the oxidation of **1′** leads principally to the oxidation of the double bond C^7–C^{14}. Should the 0.215 spin density on C^{14} be sufficient to allow dimerization at this carbon, the steric hindrance around C^{14} may be strong enough to explain why coupling was not observed. Moreover, the spin density on the carbons C^2 and

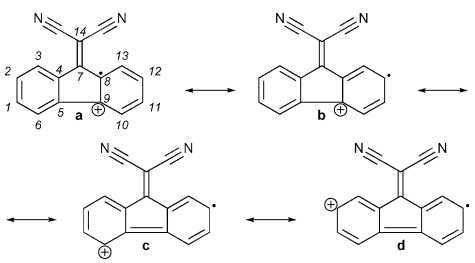

Scheme 4 Resonance structures of the radical cation of **3**.

 This journal is © the Royal Society of Chemistry and the Centre National de la Recherche Scientifique 2007

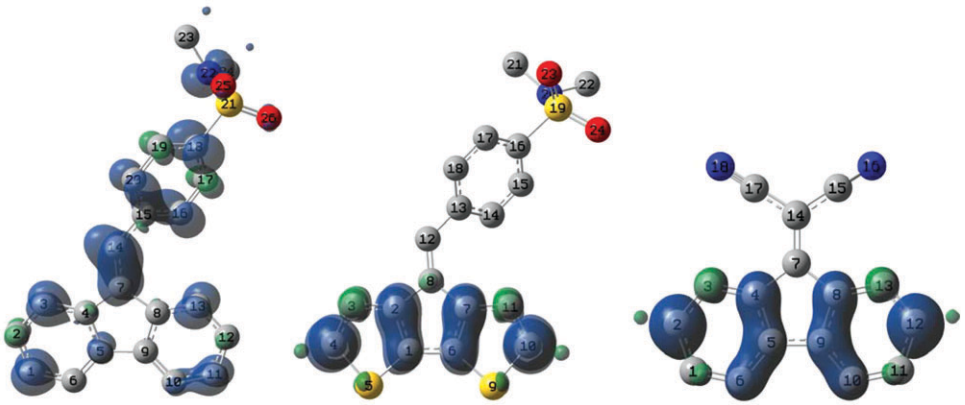

Fig. 5 Unpaired electron density surface from spin SCF density for radical cation of **1′**, **2′** and **3** (0.002 *e* Å^{-3}, B3LYP/6-31G(d)). (Hydrogen atoms omitted for clarity).

Published on 28 June 2007 on http://pubs.rsc.org | doi:10.1039/B704340F
Downloaded by University of Belgrade on 01 January 2013

C^{12}, classically involved in C–C coupling along anodic oxidations, is nearly equal to zero. The 0.122 au partial charge found on C^7 reflects a notable contribution of mesomers **a**–**c** (Scheme 2). The 0.160 au spin density calculated for C^{18} is in agreement with mesomer **c** (Scheme 2). Furthermore, the contributions of regioisomeric mesomers **a′**–**c′** are accounted for by spin densities of 0.136 and 0.112 au found, respectively on C^7 and C^1.

The unpaired electron spin density of the **2′** radical cation appears distributed only on the bithiophene part of the molecule. The highest unpaired electron spin density is located on carbons C^4 and C^{10} which are involved in the coupling during polymerization, implying an important contribution of mesomers **c**–**f** to the "real" structure of the radical cation (Scheme 3). Compared with the **1′** radical cation, the positive charge looks more uniformly distributed over the whole skeleton, reflecting the contribution of mesomers **a**–**f**. These results confirm what was discussed previously with the analysis of the structure modifications.

Results reported in both Fig. 5 and Table 3 fully support the assumption based on the structural analysis of the **3** radical cation which indicated that the quinoidal mesomer **d** (Scheme 4) should afford a preponderant contribution to the "real" radical cation **3**. Indeed, the C^2/C^{12} carbons bear the highest spin density but also show the largest atomic charge variations. These facts are in full agreement with the quinoidal mesomer **d** (Scheme 4). The 0.28 au spin density that is calculated for C^2/C^{12} is much higher than the small β spin density (~ -0.05 au) found on the same centers of the **1′** radical cation. On the other hand, this 0.28 au spin density is close to the 0.318 au found on the C^4/C^{10} atoms of the CPDT analogue **2′** radical cation. In both cases, these carbons are involved in the coupling during polymerization.

Conclusions

The comparative study of the geometrical changes occurring when going from neutral molecules to radical cations of **1′**, **2′** and **3** and of the spin density distribution in the radical cations, allows understanding of the contrasting behaviour of **2′** (and **3**) *vs.* **1′**. The radical is essentially located on the tricyclic aromatic system of **2′** and **3**, whereas for **1′** the radical seems to be delocalized on the whole structure. Scrutiny of changes occurring in radical cations **2′** and **3** allows emphasis of the differences in behaviour which are closely correlated to the electrochemical properties.

A global view of both spin and charge distributions is obtained by partitioning the monomers into three domains:

Table 3 DFT computed Mulliken spin densities for **1′**, **2′** and **3** radical cations and variations of CHelpG charges between **1′**, **2′** and **3** radical cations and neutral molecules (au, B3LYP/6-31G(d))[a,b]

1′ Radical cation			**2′** Radical cation			**3** Radical cation		
Atom no.	Spin density	$\Delta\delta$	Atom no.	Spin density	$\Delta\delta$	Atom no.	Spin density	$\Delta\delta$
C1	**0.112**	**0.123**	C1	**0.114**	−0.018	C2	***0.280***	**0.199**
C7	**0.136**	**0.122**	C2	**0.229**	**0.166**	C4	**0.156**	**0.111**
C11	0.078	**0.118**	C4	***0.318***	**0.160**	C5	**0.116**	0.026
C13	0.090	**0.116**	S5	−0.042	**0.121**	C7	−0.041	**−0.121**
C14	***0.215***	0.077	C7	**0.233**	**0.150**	C8	**0.156**	0.119
C18	**0.160**	0.018	C8	−0.052	**−0.144**	C9	**0.116**	0.026
			S9	−0.039	**0.115**	C11	−0.041	0.027
			C10	***0.326***	**0.150**	C12	***0.280***	**0.209**
			C12	0.003	**0.150**	C14	0.008	**0.130**
			C13	−0.002	**−0.154**			
			C18	−0.002	**0.106**			

[a] Results are given for atoms for which either spin density or CHelpG charge variation ($\Delta\delta$) are larger than 0.1 (in bold; the largest spin density is further indicated in bold italic). [b] Spin densities and charges summed up with bound H.

View Article Online

Table 4 DFT computed Mulliken spin densities and variations of CHelpG charges after partitioning of monomers **1′**, **2′** and **3** into three areas (au, B3LYP/6-31G(d))

		Fluorene or CPDT (tricyclic arom.)	Methylidene bridge (C^{12} or C^{14})	Benzene-sulfonamide
Spin density	**1′**	0.455	0.215	0.330
	2′	1.003	0.003	−0.006
	3	0.991	0.008	—
$\Delta\delta$	**1′**	*0.546*	*0.077*	*0.377*
	2′	*0.715*	*0.150*	*0.135*
	3	*0.757*	*0.130*	—

the CPDT or fluorene parts, the methylidene bridge and the benzenesulfonamide group. This way, Table 3 may be condensed into Table 4.

It appears from Table 4 that 100% of the spin density of **2′** is located on the CPDT area of the radical cation. The same is observed for the fluorene area of **3** radical cation. These calculations are in complete agreement with the preliminary conclusions drawn from the initial study of the geometrical parameters. Consequently, assuming an RC–RC mechanism of electropolymerization, the formation of a dimer dication from the coupling of radical cations **2′** at C^4/C^{10} positions (**c**–**f** mesomers, Scheme 3) should easily take place. In the same way, the coupling of radical cations **3** at C^2/C^{12} positions (**b**–**d** mesomers, Scheme 4) is thus rationalized.

As for **1′**, the delocalization of both spin and charge over the whole skeleton is clearly reflected by the values reported in Table 4. As a consequence, because of the lack of a well-localized spin density, radical coupling should be far less easy than in the case of **2′** or **3**.

Thus, these DFT calculations point out that different locations for the electronic perturbation induced by one-electron oxidation correspond to fundamentally different routes for radical cation evolution.

Acknowledgements

Computations have been carried out at the Centre de Ressources Informatiques de Haute-Normandie (CRIHAN, Saint-Etienne-du-Rouvray, France). The authors wish to acknowledge the Universities of Le Mans and Rennes 1 and the CNRS (UMR 6011 and 6510) for financial support and technical assistance.

References

1 R. Xia, G. Heliotis and D. D. C. Bradley, *Synth. Met*., 2004, **140**(2–3), 117.
2 T. W. Lee, O. O. Park, H. N. Cho and Y. C. Kim, *Cur. Appl. Phys*., 2001, **1**(4/5), 363.
3 J. Rault-Berthelot and E. Raoult, *Synth. Met*., 2001, **123**, 101.
4 (*a*) A. Berthelot, G. Marchand, H. T. Huynh and J. F. Pilard, *Electrochem. Commun*., 2001, **3**, 557; (*b*) G. Marchand, J. F. Pilard and J. Simonet, *Tetrahedron Lett*., 2000, **41**, 883.
5 J. F. Pilard, C. Cougnon, J. Rault-Berthelot, A. Berthelot, C. Hubert and K. Tran, *J. Electroanal. Chem*., 2004, **568**, 195–201.
6 J. Rault-Berthelot, C. Roze and M. M. Granger, *J. Electroanal. Chem*., 1997, **436**, 85.
7 *MacSpartan '02*, Wavefunction, Inc., 18401 Von Karman Avenue, Suite 370, Irvine, CA 92612 USA, http://www.wavefun.com.
8 M. J. Frisch, G. W. Trucks, H. B. Schlegel, G. E. Scuseria, M. A. Robb, J. R. Cheeseman, V. G. Zakrzewski, J. A. Montgomery, Jr, R. E. Stratmann, J. C. Burant, S. Dapprich, J. M. Millam, A. D. Daniels, K. N. Kudin, M. C. Strain, O. Farkas, J. Tomasi, V. Barone, M. Cossi, R. Cammi, B. Mennucci, C. Pomelli, C. Adamo, S. Clifford, J. Ochterski, G. A. Petersson, P. Y. Ayala, Q. Cui, K. Morokuma, D. K. Malick, A. D. Rabuck, K. Raghavachari, J. B. Foresman, J. Cioslowski, J. V. Ortiz, B. B. Stefanov, G. Liu, A. Liashenko, P. Piskorz, I. Komaromi, R. Gomperts, R. L. Martin, D. J. Fox, T. Keith, M. A. Al-Laham, C. Y. Peng, A. Nanayakkara, C. Gonzalez, M. Challacombe, P. M. W. Gill, B. G. Johnson, W. Chen, M. W. Wong, J. L. Andres, M. Head-Gordon, E. S. Replogle and J. A. Pople, *GAUSSIAN 98 (Revision A111)*, Gaussian, inc., Pittsburgh, PA, 2001.
9 E. M. Genies, G. Bidan and A. F. Diaz, *J. Electroanal. Chem*., 1983, **149**, 101.
10 J. C. Lacroix, F. Maurel and P. C. Lacaze, *J. Am. Chem. Soc*., 2001, **123**, 1989.
11 R. J. Waltman and J. Bargon, *Tetrahedron*, 1984, **40**, 3963.
12 J. R. Smith, P. A. Cox, S. A. Campbell and N. M. Ratcliffe, *J. Chem. Soc., Faraday Trans*., 1995, **91**, 2331.
13 M. Fréchette, M. Belletête, J. Y. Bergeron, G. Durocher and M. Leclerc, *Macromol. Chem. Phys*., 1997, **198**, 1709.
14 J. C. Lacroix, R. J. Valente, F. Maurel and P. C. Lacaze, *Chem.–Eur. J*., 1998, **4**, 1667.
15 T. Hayakawa, K. I. Fukukawa, M. Morishima, K. Takeuchi, M. Asai, S. Ando and M. Ueda, *J. Polym. Sci., Part A: Polym. Chem*., 2001, **39**, 2287.
16 S. Ando and M. Ueda, *Synth. Met*., 2002, **129**, 207.
17 M. Yurtsever and E. Yurtsever, *Polymer*, 2002, **43**, 6019.
18 M. Yurtsever and E. Yurtsever, *Polymer*, 2004, **45**, 9039.
19 M. Satoh, K. Imanishi and K. Yoshino, *J. Electroanal. Chem*., 1991, **317**, 139.
20 Y. Wei, C. C. Chan, J. Tian, G. W. Jang and K. F. Hsueh, *Chem. Mater*., 1991, **3**, 888.
21 H. Talbi, G. Monard, M. Loos and D. Billaud, *Theochem*., 1998, **434**, 129.
22 H. Talbi, G. Monard, M. Loos and D. Billaud, *Synth. Met*., 1999, **101**, 115.
23 E. Yurtsever, *Synth. Met*., 2001, **119**, 227.
24 J. C. Lacroix, P. Garcia, J. P. Audiere, R. Clement and O. Kahn, *New J. Chem*., 1990, **14**, 87.
25 J. C. Lacroix, M. Mostefai, G. Havard, M. C. Pham, J. P. Doucet and P. C. Lacaze, *New J. Chem*., 1995, **19**, 979.
26 J. C. Lacroix, G. Harvard, J. J. Aaron, K. Taha-Bouamri and P. C. Lacaze, *Struct. Chem*., 1997, **8**, 177.
27 G. D'Aprano, E. Proynov, M. Leboeuf, M. Leclerc and D. R. Salahub, *J. Am. Chem. Soc*., 1996, **118**, 9736.
28 R. N. Adams, *Acc. Chem. Res*., 1969, **2**, 175.
29 J. F. Ambrose and R. F. Nelson, *J. Electrochem. Soc*., 1968, **115**, 1159.
30 R. M. Dessau and S. Shih, *J. Chem. Phys*., 1970, **53**, 3169.
31 K. Sanechika, T. Yamamoto and A. Yamamoto, *J. Polym. Sci., Polym. Lett. Ed*., 1982, **20**, 365.
32 R. J. Waltman, A. F. Diaz and J. Bargon, *J. Phys. Chem*., 1984, **88**, 4343.
33 R. J. Waltman and J. Bargon, *Can. J. Chem*., 1986, **64**, 76.
34 J. P. Ruiz, M. B. Gieselman, K. Nayak, D. S. Marynick and J. R. Reynolds, *Synth. Met*., 1989, **28**, 481.
35 M. Karelson and M. C. Zerner, *Chem. Phys. Lett*., 1994, **224**, 213.
36 M. Fréchette, M. Belletête, J. Y. Bergeron, G. Durocher and M. Leclerc, *Synth. Met*., 1997, **84**, 223.
37 M. Mathis, W. Harsha, T. W. Hanks, R. D. Bailey, G. L. Schimek and W. T. Pennington, *Chem. Mater*., 1998, **10**, 3568.
38 J. R. Smith, P. A. Cox, N. M. Ratcliffe and S. A. Campbell, *Trans. Inst. Met. Finish*., 2002, **80**, 52.
39 H. Sabzyan and A. Omrani, *J. Phys. Chem. A*, 2003, **107**, 6476.
40 H. Sabzyan and H. Nikoofard, *Chem. Phys*., 2004, **306**, 105.
41 P. Audebert, J. M. Catel, G. Le Coustumer, V. Duchenet and P. Hapiot, *J. Phys. Chem. B*, 1998, **102**, 8661.
42 Spin densities were computed following both Mulliken and NPA schemes. Similar values were obtained thus, only the Mulliken spin densities are shown in Tables 3 and 4. The small spin densities on H atoms are condensed with the corresponding C atoms spin densities. See ESI‡.

Published on 28 June 2007 on http://pubs.rsc.org | doi:10.1039/B704340F
Downloaded by University of Belgrade on 01 January 2013

 This journal is © the Royal Society of Chemistry and the Centre National de la Recherche Scientifique 2007

View Article Online

43 C. M. Breneman and K. B. Wiberg, *J. Comput. Chem.*, 1990, **11**, 361.
44 Atomic charges computed following NPA[45] and MKS[46] schemes were found very close to the CHelpG charges (see ESI‡).
45 Computed within Gaussian98 with the program: NBO Version 3.1, E. D. Glendening, A. E. Reed, J. E. Carpenter and F. Weinhold.
46 B. H. Besler, K. M. Merz, Jr and P. A. Kollman, *J. Comput. Chem.*, 1990, **11**, 431.

Published on 28 June 2007 on http://pubs.rsc.org | doi:10.1039/B704340F
Downloaded by University of Belgrade on 01 January 2013